ESTIMATION OF EVAPORATION USING THE SURFACE ENERGY BALANCE SYSTEM (SEBS) AND NUMERICAL MODELS

A. Ershadi[1], M.F. McCabe[1], J.P. Evans[1], J.P. Walker[2], R. Pipunic[3]

1 The University of NSW, Sydney, Australia – (a.ershadi,mmccabe,Jason.evans@unsw.edu.au)
2 Monash University, Clayton, Australia – jeff.walker@monash.edu
3 University of Melbourne, Melbourne, Australia – robp@unimelb.edu.au

Abstract – This study estimates evaporation using the Surface Energy Balance System (SEBS) method over an agricultural region in the Murrumbidgee Irrigation Area of NSW, Australia. Evaporation is estimated as latent heat flux using the standard Monin-Obukhov Similarity Theory (MOST) equations of SEBS and meteorological observations form an eddy-covariance system. Landsat and MODIS satellite data coincident with the period of in-situ flux measurements are used to examine the spatial variability of evaporation measurements. To extend the investigation, atmospheric forcing data from recent simulations of the Weather Research and Forecasting (WRF) model are used. A comparison at the point scale is made between observed eddy-covariance, modeled WRF predictions, and calculated SEBS values. In addition, the spatial variability of evaporation from the Landsat and MODIS images are compared against WRF results. Results show good estimation of the sensible heat flux using Landsat, MODIS, and WRF data, but estimation of the latent heat flux are not comparable with observations due to non-closure issues.

Keywords: Evapotranspiration, Remote Sensing, Thermal Images, NWP, WRF, SEBS

1. INTRODUCTION

Evapotranspiration (ET) is an important component of the hydrologic cycle. Accurate estimates of the surface heat fluxes would enable improved understanding of the hydrologic processes and provides better hydrologic modeling and water resources management capabilities. However, the complexity of the evapotranspiration process and a lack of parametric information required by available models, particularly at appropriate spatial and temporal scales, makes ET estimation difficult [*Brutsaert*, 1982].

Satellite images provide a valuable source of data for hydrologic modeling. Thermal images can be used in estimation of ET while other visible and near infrared bands are useful to derive vegetation structure and other land surface parameters. In this study, images from the Landsat satellite and Moderate Resolution Imaging Spectroradiometer (MODIS) on-board the Terra satellite are used for estimation of ET via the Surface Energy Balance System (SEBS) interpretive model [*Su*, 2002]. Monin-Obukhov Similarity Theory (MOST) [*Monin and Obukhov*, 1945] is explicitly incorporated into SEBS for flux estimation. Data from both a ground based meteorological station located in the study area and simulations from the Weather Research and Forecasting (WRF) model [*Evans and McCabe*, 2010] for South-East Australia provide the needed meteorological forcing.

2. STUDY AREA AND DATA

The focus of the study is a small region in the Murrumbidgee Irrigation Area in NSW, Australia (see Fig. 1). An eddy-covariance (EC) instrument was installed in a tomato field for continuous flux measurement during an intensive field campaign. Measurements at the site included all radiation terms, sensible and latent heat fluxes, and meteorologic parameters averaged to 1 hour time steps after required coordinate conversions and corrections. No soil heat flux data were available, so approximations have been used for this variable. The EC system was approximately 2 metres above the plant canopy and the plants were estimated to be 50cm high in furrows approximately 2 meters apart.

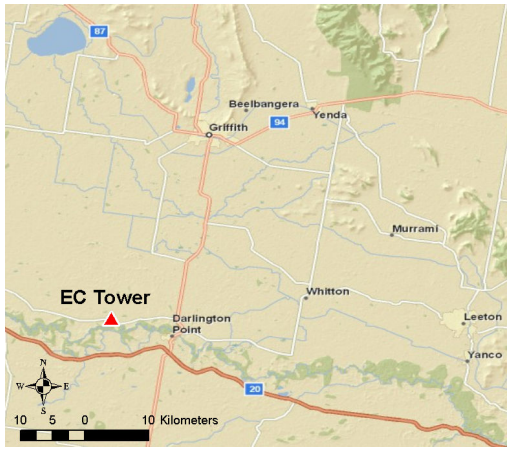

Fig. 1: Location of the EC tower

A Landsat TM 5 image (Path 92, Row 84) for 1 Dec 2009 (DOY 335) at 23:53 UTC (2 Dec 2009 at 10:53 local time) was selected, with flux tower data at 11 AM local time used for comparison. An area of around 9×9 km centred on the flux tower was extracted from the Landsat image and all bands averaged to a common 60 meter spatial resolution grid.

Land surface temperature from the MODIS derived MOD11 products for the same day of the Landsat image at 23:30 UTC were used to estimate sensible and latent heat fluxes. Atmospheric profiles from MOD07 products provided information for atmospheric correction of the Landsat image using MODTRAN 5 [*Berk et al.*, 2008; *Berk et al.*, 2009].

Atmospheric forcing data for calculation of sensible heat flux were also derived from the Weather Research and Forecast (WRF) model [*NCAR*, 2009] simulation of the Murray Darling Basin [*Evans and McCabe*, 2010], which reproduces hydrometeorological conditions over South-East Australia for more than 24 years at a 10 km horizontal grid. Air temperature, wind speed, humidity, and air pressure were extracted from the surface atmospheric layer of WRF.

3. METHODOLOGY

Estimation of land surface parameters

LAI and albedo were calculated based on the Normalized Difference Vegetation Index (NDVI) following the

methodology of *Wang et al.* [2008]. For estimation of NDVI, use is made of bands 3 and 4 of the Landsat image following relationship of *Sobrino et al.* [2004]. For estimation of fractional vegetation cover, the methodology by *Jiménez-Muñoz et al.* [2009] was used. Also, emissivity was calculated using the methodology of *Sobrino et al.* [2004]. Zero-plane displacement height (d_0) and roughness length parameters for momentum and heat transfer (z_{0m} and z_{0h}), were derived using the methodology originally developed by *Massman* [1997] and *Su et al.* [2001].

As information on the vegetation height for all parts of the study area (except for the tomato field) are not available, z_{0m} was first calculated using a simple formula [*Allen et al.*, 2007] as $z_{0m} = 0.018 \times LAI$, with vegetation height estimated as $h_c = z_{0m}/0.136$. Next, using WRF meteorological outputs, the methodology of *Su et al.* [2001] was applied to derive all roughness parameters.

Digital numbers in all bands of the Landsat image were converted to top of atmosphere (TOA) values and then to reflectance and land surface temperature following the methodology of *Chander et al.* [2007]. All bands were atmospherically corrected using MODTRAN 5 with atmospheric profiles derived from MOD07 products as noted previously.

Estimation of fluxes

In SEBS, MOST flux-gradient functions provide the basis for estimation of sensible heat flux (H) as the transfer of heat from the land (canopy) to a level in the atmosphere. The functions are defined as:

$$u_a = \frac{u_*}{\kappa}\left[\ln\left(\frac{z-d_0}{z_{0m}}\right) - \Psi_m\left(\frac{z-d_0}{L}\right) + \Psi_m\left(\frac{z_{0m}}{L}\right)\right] \quad (1)$$

$$\theta_s - \theta_a = \frac{H}{\kappa u_* \rho c_p}\left[\ln\left(\frac{z-d_0}{z_{0h}}\right) - \Psi_h\left(\frac{z-d_0}{L}\right) + \Psi_h\left(\frac{z_{0h}}{L}\right)\right] \quad (2)$$

where L is known as the Obukhov stability length, and is defined as:

$$L = -\frac{\rho c_p u_* \theta_v}{\kappa g H} \quad (3)$$

Here H is the sensible heat flux [Wm^{-2}]; ρ is air density; κ is von Karman's constant (0.4); u_* is friction velocity; d_0 is zero-plane displacement height; z_{0m} and z_{0h} are roughness lengths for momentum and heat transfer; z is height above ground level; u_a is mean wind speed; θ_s is the land surface potential temperature in K; θ_a is mean air potential temperature in K; θ_v is mean air virtual potential temperature in K; and Ψ_m and Ψ_h are integrated forms of the MOST stability correction functions for momentum and heat transfer. It should be noted that these formula are not stand-alone and to quantify H, one needs to solve all three equations iteratively. Here, for estimation of Ψ_m and Ψ_h in stable condition, the formulations proposed by *Beljaars and Holtslag* [1991] and evaluated by *van den Hurk and Holtslag* [1997] were used, while for unstable conditions the equations developed by *Brutsaert* [2005] were employed.

For estimation of net radiation (R_n) at the image scale, observations of shortwave and longwave downward radiation from the EC tower were used. Shortwave upward radiation at image scale was estimated using the albedo (α) layer, while longwave upward radiation was calculated using the Stefan-Boltzmann law with emissivity and land surface temperature from the Landsat image.

As there were no soil heat flux observations, G_0 was calculated using an equation suggested by *Su* [2002] as

$$G_0 = R_n\left[0.05 + 0.265(1 - f_c)\right], \quad (4)$$

where f_c is fractional vegetation cover. Finally, the latent heat flux (λE) calculated as the residual term in the general energy balance equation ($\lambda E = R_n - G_0 - H$).

Sensible heat flux was calculated at both tower and image scales using the above methodology in four different scenarios, as shown in Table 1.

Table 1: Definition of scenarios in estimation of H

Scenario	T_s	T_a, u_a, q_a	Scale
TWTW	Tower	Tower	Point
TMTW	Landsat	Tower	Point
TMWF	Landsat	WRF	Image
MDWF	MODIS	WRF	Image

In the TWTW scenario, both land surface temperature and atmospheric forcing data were obtained from EC tower observations. In both the TMTW and TMWF scenarios, land surface temperature were obtained from the Landsat (TM) image, but atmospheric forcing data were obtained from the tower (TW) for the TMTW scenario and WRF model (WF) for the TMWF scenarios. In the last scenario (MDWF), land surface temperature was obtained from MODIS MOD11 data, but with atmospheric forcing obtained from the WRF model. The first two scenarios in Table 1 are at point (EC tower) scale, while the remainders are at Landsat image scale. For all scenarios, h_c, d_0, z_{0m}, and z_{0h} were obtained from Landsat NDVI, with z_{0h} updated based on the atmospheric forcing. As there was no observation of T_s at the EC tower, in the TWTW scenario T_s is calculated by inverting the Stefan-Boltzmann equation using the emissivity calculated from the Landsat image.

4. RESULTS AND DISCUSSION

For the point scale comparisons, Table 2 presents the results of the fluxes derived from the three point scale scenarios at the tower. In the TMTW and TMWF scenarios, H and λE were extracted from the pixel containing the tower. As can be seen, estimation of H in the TMWF scenario worked as well as the tower based retrievals (TWTW scenario) and clearly shows that WRF atmospheric outputs represented observed tower values. However, WRF output of H is different from the tower observations and three scenarios shown in Table 1, which might be due to high T_s in WRF (5.3 °C warmer than tower T_s). Other possible reasons for the WRF discrepancy in H and λE compared to the EC tower site may be related to (a) the pixel size difference (10 km for WRF); (b) the land-use and vegetation type difference (dryland cropland and pasture in WRF); and (c) the difference in quantification of fluxes as determined in the NOAH Land Surface Model [*Chen*, 2007] where a combined approach of water and energy balance was employed.

Table 2: Flux terms as observed in ET tower, resulted from WRF and simulated in first three scenarios

	Tower Observed	TWTW	TMTW	TMWF	WRF output
H	119.4	166.7	184.9	174.5	431
λE	204.6	400	382	392.5	19
H_{diff}	-	-47.3	-65.5	-55.1	-312
λE_{diff}	-	-195.4	-177.4	-187.9	185.6

The λE_{diff} in all scenarios is very high and is mainly due to the non-closure sources and in estimation of G_0 using equation (4).

In image scale, results from the TMWF scenario for H and λE are shown in Fig. 2 and Fig. 3 illustrating the spatial distribution of sensible and latent heat flux.

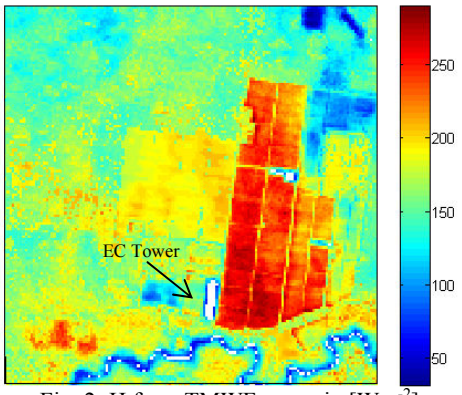

Fig. 2: H from TMWF scenario [Wm^{-2}]

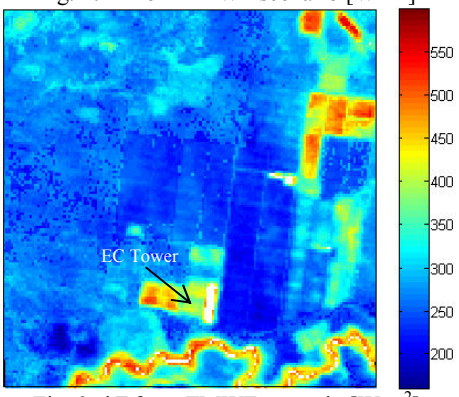

Fig. 3: λE from TMWF scenario [Wm^{-2}]

In the MDWF scenario, MOD11 land surface temperature from MODIS was used in estimation of H and λE with atmospheric forcing from WRF and roughness parameters from Landsat. The T_s in MOD11 is not accurate here as the study area is located at the edge of the MODIS image and satellite viewing angle is high. Also, the MODIS resolution is bigger than 1km and therefore is significantly larger than that for Landsat (60m), with the accuracy of T_s expected to be affected by heterogeneity of the surface. Maps of T_s for Landsat and MODIS images are presented in Fig. 4 and Fig. 5. Note that due to the sinusoidal projection of the MODIS image, the distance between the pixels is irregular. Instead of reprojection and resampling, the nearest MODIS pixel corresponding to each Landsat pixels is determined, resulted in a Thiessen polygon form of MODIS pixels as seen in Fig. 5. H and λE resulting from the MDWF scenario are shown in Fig. 6 and Fig. 7.

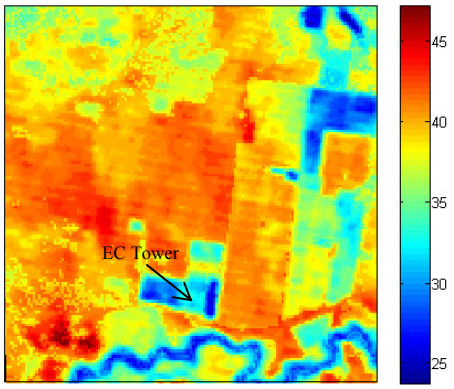

Fig. 4: Land surface temperature in Landsat image (°C)

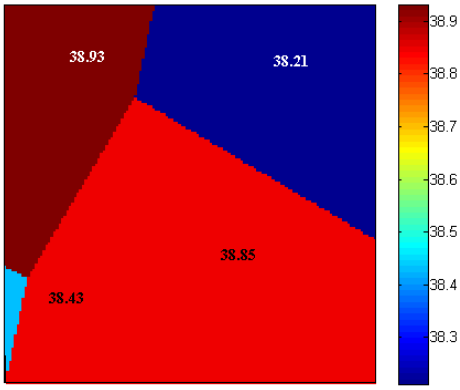

Fig. 5: Land surface temperature in MODIS image (°C)

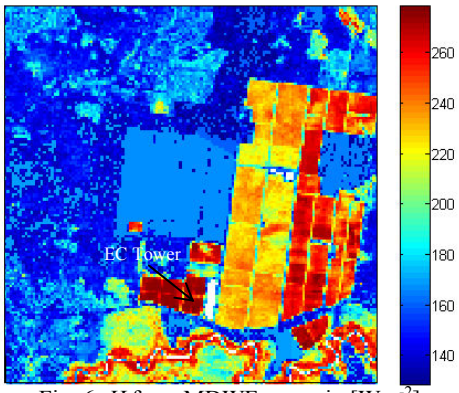

Fig. 6: H from MDWF scenario [Wm^{-2}]

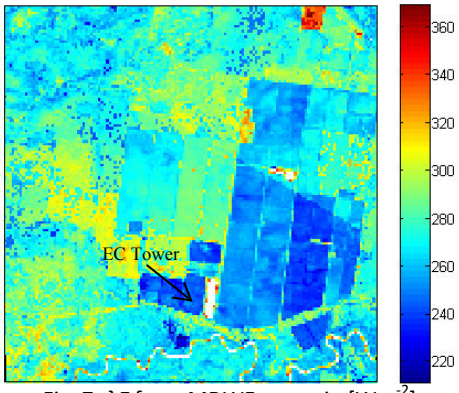

Fig. 7: λE from MDWF scenario [Wm^{-2}]

A statistical summary of T_s, H, λE, G_0, and R_n for Landsat and MODIS (TMWF and MDWF scenarios) is shown in Table 3. Mean T_s values for Landsat and MODIS across the entire study area are in good agreement, with a 0.5 °C difference. However, the standard deviations in T_s were large due to the different sensor characteristics, spectral responses

and spatial resolution. As such, MODIS was not able to capture the variability of the land surface temperature evident in the scene.

Table 3: Mean (μ) and standard deviation (σ) of T_s and flux terms for TMWF and MDWF scenarios

	Stat.	TMWF	MDWF
T_s	μ	38.2	38.7
	σ	3.7	0.3
H	μ	171	181
	σ	38	41
λE	μ	276	272
	σ	77	18
G_0	μ	179	178
	σ	22	24
R_n	μ	635	632
	σ	37	23

Both the mean and standard deviation of H in Landsat and MODIS (in TMWF and MDWF scenarios) for the entire study area are very close, indicating that introducing roughness length parameters (h_c, d_0, z_{0m}, z_{0h}) aids in better estimation of sensible heat flux using MOST for MODIS. However, while mean values for λE in Landsat and MODIS are similar, their standard deviations are different, which might be associated to the effect of low σ of T_s in R_n and consequently into λE via the energy balance equation. These results, especially the similarity in derived H for MODIS and Landsat, have potential application in disaggregation of thermal images and flux products, which is the focus of current investigations.

ACKNOWLEDGEMENT

Funding for this research is provided by Australian Arc-Linkage Project LP0989441 with support of the Department of Primary Industries, Tatura as an Industry partner. We thank Dr. Fuqin Li from Geoscience Australia for her help in atmospheric correction of Landsat images.

5. REFERENCES

Allen, R. G., M. Tasumi, and R. Trezza (2007), Satellite-Based Energy Balance for Mapping Evapotranspiration with Internalized Calibration (METRIC)---Model, *Journal of Irrigation and Drainage Engineering*, *133*(4), 380-394.

Beljaars, A. C. M., and A. A. M. Holtslag (1991), Flux Parameterization over Land Surfaces for Atmospheric Models, *Journal of Applied Meteorology*, *30*(3), 327-341.

Berk, A., G. P. Anderson, P. K. Acharya, and E. P. Shettle (2008), MODTRAN®5.2.0.0 Uers's Manual, edited, p. 98, SPECTRAL SCIENCES, INC.

Berk, A., P. Acharya, G. Anderson, and B. Gossage (2009), Recent developments in the MODTRAN atmospheric model and implications for hyperspectral compensation, paper presented at Geoscience and Remote Sensing Symposium,2009 IEEE International,IGARSS 2009.

Brutsaert, W. (1982), *Evaporation Into the Atmosphere : theory, history, and applications*, 299 pp., Reidel Publishing, Dordrecht etc.

Brutsaert, W. (2005), *Hydrology : An Introduction*, 605 pp., Cambridge University Press, Cambridge.

Chander, G., and B. Markham (2003), Revised Landsat-5 TM radiometric calibration procedures and postcalibration dynamic ranges, *Geoscience and Remote Sensing, IEEE Transactions on*, *41*(11), 2674-2677.

Chander, G., B. L. Markham, and J. A. Barsi (2007), Revised Landsat-5 Thematic Mapper Radiometric Calibration, *Geoscience and Remote Sensing Letters, IEEE*, *4*(3), 490-494.

Chen, F. (2007), The Noah Land Surface Model in WRF; A Short Tutorial, edited, NCAR, RAL.

Evans, J. P., and M. F. McCabe (2010), Regional climate simulation over Australia's Murray-Darling basin: A multitemporal assessment, *J. Geophys. Res.*, *115*(D14), D14114.

Jiménez-Muñoz, J., J. Sobrino, A. Plaza, L. Guanter, J. Moreno, and P. Martinez (2009), Comparison Between Fractional Vegetation Cover Retrievals from Vegetation Indices and Spectral Mixture Analysis: Case Study of PROBA/CHRIS Data Over an Agricultural Area, *Sensors*, *9*(2), 768-793.

Massman, W. J. (1997), An Analytical One-Dimensional Model of Momentum Transfer by Vegetation of Arbitrary Structure, *Boundary-Layer Meteorology*, *83*(3), 407-421.

Monin, A. S., and A. M. Obukhov (1945), Basic laws of turbulent mixing in the surface layer of the atmosphere, *Tr. Akad. Nauk SSSR Geophiz. Inst.*, *24*(151), 163-187.

NCAR (2009), Weather Research & Forecast WRF - ARW Version 3 Modeling System User's Guide, edited.

Sobrino, J. A., J. C. Jiménez-Muñoz, and L. Paolini (2004), Land surface temperature retrieval from LANDSAT TM 5, *Remote Sensing of Environment*, *90*(4), 434-440.

Su, Z. (2002), The Surface Energy Balance System (SEBS) for estimation of turbulent heat fluxes, *Hydrol. Earth Syst. Sci.*, *6*(1), 85-100.

Su, Z., T. Schmugge, W. P. Kustas, and W. J. Massman (2001), An Evaluation of Two Models for Estimation of the Roughness Height for Heat Transfer between the Land Surface and the Atmosphere, *Journal of Applied Meteorology*, *40*(11), 1933-1951.

van den Hurk, B. J. J. M., and A. A. M. Holtslag (1997), On the bulk parameterization of surface fluxes for various conditions and parameter ranges, *Boundary-Layer Meteorology*, *82*(1), 119-133.

Wang, L., G. N. Parodi, and Z. Su (2008), SEBS Module BEAM: A Practical Tool for Surface Energy Balance Estimates from Remote Sensing Data, in *The 2nd MERIS-(A) ATSR Workshop*, edited, ESRIN, Frascati, Italy.